Engineering 29 (2023) 95–109

Contents lists available at ScienceDirect

Engineering

journal homepage: www.elsevier.com/locate/eng

Research
Medical Engineering—Article

Biosynthesis and Immunological Evaluation of a Dual-Antigen Nanoconjugate Vaccine Against *Brucella melitensis*

Jing Huang [a,b,c,#], Yufei Wang [d,#], Kangfeng Wang [a,e], Shulei Li [a,d], Peng Sun [a], Yan Guo [a], Jiankai Liu [b], Ruifu Yang [c], Ming Zeng [b,*], Chao Pan [a,*], Hengliang Wang [a,*], Li Zhu [a,*]

[a] *State Key Laboratory of Pathogen and Biosecurity, Beijing Institute of Biotechnology, Beijing 100071, China*
[b] *Beijing Minhai Biotechnology Co., Ltd., Beijing 102600, China*
[c] *State Key Laboratory of Pathogen and Biosecurity, Beijing Institute of Microbiology and Epidemiology, Beijing 100071, China*
[d] *The Third Medical Center, PLA General Hospital, Beijing 100039, China*
[e] *College of Life Science, Hebei University, Baoding 071002, China*

ARTICLE INFO

Article history:
Received 26 October 2022
Revised 26 January 2023
Accepted 19 April 2023
Available online 12 May 2023

Keywords:
Protein glycan coupling technology (PGCT)
Dual-antigen
Nanoconjugate vaccine
Brucella melitensis

ABSTRACT

Brucellosis, caused by *Brucella*, is one of the most common zoonosis. However, there is still no vaccine for human use. Although some live attenuated vaccines have been approved for animals, the protection effect is not ideal. In this study, we developed a dual-antigen nanoconjugate vaccine containing both polysaccharide and protein antigens against *Brucella*. First, the antigenic polysaccharide was covalently coupled to the outer membrane protein Omp19 using protein glycan coupling technology, and then it was successfully loaded on a nano-carrier through the SpyTag/SpyCatcher system. After confirming the efficient immune activation and safety performance of the dual-antigen nanoconjugate vaccine, the potent serum antibody response against the two antigens and remarkable protective effect in non-lethal and lethal *Brucella* infection models were further demonstrated through different routes of administration. These results indicated that the dual-antigen nanoconjugate vaccine enhanced both T helper 1 cell (Th1) and Th2 immune responses and protected mice from *Brucella* infection. Furthermore, we found that this protective effect was maintained for at least 18 weeks. To our knowledge, this is the first *Brucella* vaccine bearing diverse antigens, including a protein and polysaccharide, on a single nanoparticle. Thus, we also present an attractive technology for co-delivery of different types of antigens using a strategy applicable to other vaccines against infectious diseases.

© 2023 THE AUTHORS. Published by Elsevier LTD on behalf of Chinese Academy of Engineering and Higher Education Press Limited Company. This is an open access article under the CC BY-NC-ND license (http://creativecommons.org/licenses/by-nc-nd/4.0/).

1. Introduction

Brucellosis, one of the major zoonotic diseases, is caused by *Brucella* spp., a Gram-negative, facultative intracellular bacteria. *Brucella melitensis* (*B. melitensis*), *Brucella abortus* (*B. abortus*), and *Brucella suis* (*B. suis*) are the three most common *Brucella* pathogens and can infect both animals and humans in epidemic areas, resulting in tremendous economic losses every year [1]. Brucellosis is prevalent in the world and endangers public health. There are millions of poultry and livestock are at risk [2]. In domestic animals, brucellosis causes abortions, stillbirths, infertility, increased mortality of young livestock, longer calving intervals, reduced draught power, poor weight gain, and reduced milk production [3]. *Brucella* is a pathogen with aerosol transmission potential, and the amount of inoculant required to infect human beings is very low. It has been reported that as few as 10 to 100 organisms can cause disease in humans. Thus, *Brucella* has been classified as a severe biological threat worldwide [4]. There are more than half a million new cases of brucellosis each year, with prevalence rates in some countries exceeding 10 per 100 000 people. In particular, the incidence is higher among people who work on organized farms [5]. Traditionally, the human disease presents as a flu-like undulant fever with various clinical symptoms, including headaches, muscle pain, sweating, or chills, and may lead to severe debilitation and disability [5,6]. Moreover, due to the wide distribution of cases, misdiagnosis, and other factors, these data are greatly underestimated [1]. At present, there is no approved brucellosis

* Corresponding authors.
E-mail addresses: zengming@263.net (M. Zeng), panchaosunny@163.com (C. Pan), wanghl@bmi.ac.cn (H. Wang), jewly54@bmi.ac.cn (L. Zhu).
# These authors contributed equally to this work.

https://doi.org/10.1016/j.eng.2023.04.007
2095-8099/© 2023 THE AUTHORS. Published by Elsevier LTD on behalf of Chinese Academy of Engineering and Higher Education Press Limited Company.
This is an open access article under the CC BY-NC-ND license (http://creativecommons.org/licenses/by-nc-nd/4.0/).

vaccine used for humans. Although animal vaccines are crucial to control the infection and transmission of brucellosis, several live attenuated vaccines have shortcomings, such as causing human disease, spontaneous abortion in animals, antibiotic resistance, and insufficient protective efficacy [7].

Compared with live attenuated vaccines, subunit vaccines, which contain specific antigen components, have many advantages, such as more controlled production, higher safety, and broader applicability, as they can be used for humans and pregnant animals [8]. The success of recombinant subunit vaccines usually depends on the selection of substances with appropriate immunomodulatory properties that can induce antigen-specific immune responses [9]. For *Brucella*, several cell surface components, such as outer membrane proteins (e.g., Omp16, Omp19, and Omp31) and intracellular components (e.g., L7/L12, lumazine synthase, and Cu–Zn superoxide dismutase), have been shown to be protective antigens against *Brucella* infection in animal studies [10]. However, because of the sophisticated virulence mechanisms and strain heterogeneity of *Brucella*, adequate protection from a single antigen is not likely [11]. It has also been reported that a vaccine prepared using a recombinant Omp31 protein fusion with *Brucella* lumazine synthase as a protective antigen had better immune effects than vaccines using each individual protein as the antigen [12]. This result suggested that the choice of adequate multiple antigens and delivery through an appropriate method are very important [9].

Glycoconjugate vaccines are known as the most successful bacterial vaccines due to their ability to induce both T-cell and B-cell immune responses and long-term protection [13]. With the development of synthetic biology technology, more efficient biological methods for bacterial glycoconjugate vaccine preparation have gradually become popular [14,15]. In this method, the O-antigen polysaccharide (OPS) of a pathogenic bacteria is directly coupled to a carrier protein in an attenuated host bacteria through the catalysis of glycosyltransferase [16–18]. However, this strategy is not suitable for *Brucella* due to its high infectivity and slow growth. In our previous work, we prepared an efficient *Brucella* glycoconjugate vaccine by introducing an O-linked glycosylation system (co-expression of glycosyltransferase PglL and recombinant cholera toxin B subunit (rCTB)) into *Yersinia enterocolitica* (*Y. enterocolitica*) serotype O:9 (YeO9), a low-pathogenicity bacterium that has identical repeating units of OPS to *Brucella*. This candidate C-OPS_{Ba} provided great immune protection against *B. abortus* [19]. However, our subsequent results showed that the protective effect of this vaccine on *B. melitensis* was limited, possibly due to its different polysaccharide structure compared to YeO9 OPS. Because *B. melitensis* is the most common pathogenic species in human brucellosis [6], we hoped to develop a broader and more efficient *Brucella* vaccine encompassing *B. melitensis*.

The success of recombinant vaccines usually depends on the use of correct adjuvants to selectively induce diverse antigen-specific immune responses [9]. Nanoparticles have become an attractive platform for displaying and delivering antigens that offers many advantages, such as improving the stability of antigens; promoting uptake, processing, and presentation by antigen-presenting cells; and enhancing cross presentation, thereby promoting a specific immune response [20,21]. At present, various delivery systems, such as viral vectors, chitosan derivatives, liposomes, polymers, and inorganics, have been developed for brucellosis vaccines that showed improved effects [10]. Virus-like particles (VLPs), self-assembling nanoparticles, ferritin, and encapsulation offer several advantages as vaccine delivery systems facilitating targeted delivery due to their unique physicochemical properties [22]. Many methods have been used to display antigens on the surface of biocompatible nanoparticles. Instead of genetic fusion and chemical conjugation (e.g., cross-linking), modular construction of nanovaccines offers new routes and opportunities [23]. Generally, antigens can be attached to particles by non-covalent (e.g., biotin–avidin affinity) or covalent (e.g., Tag/Catcher systems) coupling technology [23]. In particular, the widely used SpyTag (ST)/SpyCatcher (SC) system connects antigens and nanoparticles through a stable, spontaneous isopeptide bond.

In this study, we developed a novel dual-antigen nanoconjugate vaccine against *Brucella* by covalently coupling an antigen module containing both polysaccharide (OPS) and protein antigens (Omp19) to a nanoparticle via protein glycan coupling technology (PGCT) [24] and the ST/SC system. Briefly, the PglL-based PGCT system, which co-expressed PglL and the recombinant carrier protein SC-Omp19 (a fusion protein with a sequon recognized by PglL), was introduced into the YeO9_52212Δ*rfaL* strain. With the help of PglL, bacterial OPS synthesized by the engineered host cells were linked to the carrier protein *in vivo*. Then, the purified glycosylated SC-Omp19 bearing antigenic polysaccharides was incubated with VLP nanoparticles carrying ST to generate the target bioconjugate nanovaccines via the covalent coupling of SC and ST. To our knowledge, this is the first time in which two different types of antigens were coupled by a biological method and loaded onto the same nanoparticle. After determining the antigen loading efficiency and vaccine stability, we then evaluated the enhancement of the immune response induced by the nanoconjugate vaccine by investigating the immune cells in draining lymph nodes (dLNs). After a subsequent vaccine safety evaluation, we further found that this dual-antigen nanoconjugate vaccine provided highly effective protection against *B. melitensis* in mice through various immunization routes and infection models. In particular, this efficient protection was maintained for at least 18 weeks. Thus, we have prepared a safe and efficient candidate vaccine for brucellosis. Moreover, we also provide an attractive technology for co-delivery of different types of antigens and present a strategy applicable to other diverse delivery systems.

2. Materials and methods

2.1. Ethics statement

All animal experiments were approved by and conducted in accordance with the recommendations of the Animal Care and Use Committee of the Academy of Military Medical Sciences (ethics approval code IACUC-DWZX-2021-008). All animals were housed and cared for in the Laboratory Animal Centre of the Academy of Military Medical Sciences at a constant ambient temperature ((23 ± 3) °C) and humidity (55% ± 5%). Materials such as cages, water bottles, and bedding were sterilized before use. Food, bedding, and water were changed every four days.

2.2. Bacterial strains and growth conditions

YeO9_52212 and the *B. melitensis* strain M5 (M5-90) were provided by the Institute for Communicable Disease Control and Prevention, Chinese Centre for Disease Control and Prevention, Beijing, China. *Y. enterocolitica* was cultured in Brain Heart Infusion (BHI) medium at 25 °C. *B. melitensis* strain M5-90 was cultured in Tryptic Soy Broth (TSB) medium at 37 °C. *B. melitensis* strain M5-90 is a vaccine strain currently used in China that was derived from the virulent *B. melitensis* strain M28, which was isolated from a sheep and serially passaged for 90 generations in chicken embryo fibroblasts [25,26]. The local hypersensitivity reactions are usually caused by the residual virulence and pathogenicity of the M5-90 strain [27]. Thus, reluctance to use this vaccine has led to the current resurgence of brucellosis [28]. All *Escherichia coli* (*E. coli*) strains were cultured in Luria–Bertani (LB) broth. Solid media contained 1.5% agar. To induce plasmid expression in the bacteria, cells

were cultured in the optimal culture medium until the optical density at 600 nm reached 0.6–0.8, and then cells were induced by isopropyl-*D*-thiogalactopyranoside (IPTG) to a final concentration of 1 mmol·L^{-1}. For protein expression in *Y. enterocolitica*, the cells were further cultured at 25 °C for 14 h, and in *E. coli*, the cells were further cultured at 30 °C for 12 h.

2.3. Construction of protein expressing plasmids

All the relevant plasmids used in this study are listed in Table 1 [16,29]. The gene encoding Omp19 was synthesized by GenScript (China). After amplification by polymerase chain reaction (PCR), the *omp19* gene was inserted into pET28a by restriction digestion and ligation to express polyhistidine (His)-tagged Omp19. The gene encoding the Tac promotor-DsbA signal peptide-SC-Omp19-glycosylation modification sequence 4573 was synthesized by PCR and Golden Gate Assembly. The gene fragment was then inserted into pET-PglL-CTB^{4573C} [16] by restriction digestion and ligation to replace CTB, producing the plasmid pET28a-PglL-SC-Omp19^{4573C}, which co-expressed PglL and SC-Omp19-4573. Another gene encoding SC-Omp19 was amplified from pET28a-PglL-SC-Omp19^{4573C} and inserted into pET28a by restriction digestion and ligation to construct the plasmid pET28a-SC-Omp19, which expressed the protein SC-Omp19 with a His tag. All the primers and restriction sites are listed in Table S1 in Appendix A.

2.4. Construction of a Y. enterocolitica strain 52212 rfaL knockout strain

A YeO9_52212 *rfaL* (encodes O-antigen ligase) knockout strain was constructed via the clustered regularly interspaced short palindromic repeat (CRISPR)–CRISPR-associated protein 9 (Cas9) system [29]. Briefly, pCas was introduced into YeO9_52212 competent cells by electroporation, then YeO9_52212/pCas was induced with *L*-arabinose (10 mmol·L^{-1} final concentration) for λ-red induction, and the competent cells were prepared. An N20 sequence of *rfaL* was linked to pTargetF by Golden Gate Assembly to obtain pTargetF-Δ*rfaL*. The upstream and downstream homologous arms of *rfaL* were synthesized by PCR and Golden Gate Assembly, and then pTargetF-Δ*rfaL* and the homologous arms were introduced into YeO9_52212/pCas competent cells. Colonies with the correct construct were identified via PCR and induced with IPTG (1 mmol·L^{-1} final concentration) to cure pTargetF-Δ*rfaL*. Finally, pCas in YeO9_52212Δ*rfaL* was cured by growing overnight at 37 °C. All the primers and restriction sites are listed in Table S2 in Appendix A.

2.5. Sodium dodecyl sulfate-polyacrylamide gel electrophoresis (SDS-PAGE) analysis and Western blotting

SDS-PAGE and Western blotting was performed as described previously [19]. Briefly, IPTG-induced cells (1 mL) were collected by centrifugation and resuspended in 100 μL of double distilled water (ddH_2O). The bacterial suspension or purified protein samples were mixed with an equal volume of 2× loading buffer, placed in a boiling water bath for 10 min, and separated by SDS-PAGE. Next, gels were stained with Coomassie blue or subjected to Western blotting. Horseradish peroxidase (HRP)-conjugated 6× His-tag antibody (Abmart, China) was used to detect the His-tagged proteins, 1:200 diluted YeO9 monoclonal antibody (Fitzgerald, USA) was used to detect glycoproteins, and 1:1000 diluted HRP-labeled anti-rabbit immunoglobulin G (IgG) antibody (Transgen, China) was used as the secondary antibody for the OPS-specific antibody.

2.6. Protein purification

Bacterial cells were collected after IPTG-induced expression and resuspended in Buffer A (20 mmol·L^{-1} Tris-HCl, pH 7.5, 0.5 mol·L^{-1} NaCl, and 10 mmol·L^{-1} imidazole) at a ratio of 1:10 (g·mL^{-1}). The bacteria cells were disrupted and centrifuged twice at 8000*g*, and the supernatant was collected and applied to a pre-equilibrated His-tag purification resin column. The column was washed with Buffer A using about 10 column volumes, and then the bound protein was washed with Buffer B (20 mmol·L^{-1} Tris-HCl, pH 7.5, 0.5 mol·L^{-1} NaCl, and 0.5 mol·L^{-1} imidazole). The elute was collected and concentrated using a 10- or 30-kDa-cutoff centrifugal filter (Merck, Germany) to less than 10 mL, and then was separated using size-exclusion chromatography (SEC) on a Superdex-200 column (GE Healthcare, USA). The protein of interest was collected and analyzed by 12% SDS-PAGE. The purification of bacteriophage AP205 with a ST on the N-terminus and a His tag on the C-terminus (ST-AP205) was performed as described previously [21].

2.7. Preparation of conjugated nanoparticles

Purified SC-fused protein was incubated with ST-AP205 using different molar ratios at 4 °C overnight, and then the conjugated product was detected by SDS-PAGE. In this experiment, ST-AP205 was incubated with a 1:8 molar excess of SC-Omp19 or with a 1:4 molar excess of OPS-modified SC-Omp19 (SC-Omp19-OPS) to generate AP205-Omp19 or AP205-Omp19-OPS. Then the mixture was purified using SEC on a Superdex-200 column (GE Healthcare). The protein of interest was collected and analyzed by 12% SDS-PAGE. Dynamic light scattering (DLS) analysis was performed to characterize the hydrodynamic diameter of the nanoparticles using a Zetasizer Ultra instrument (Malvern Panalytical, UK).

2.8. Animal immunization experiments

Specific-pathogen-free female BALB/c mice were purchased from Beijing Vital River Laboratory Animal Technology Co., Ltd. (China). Five- or six-week-old BALB/c mice were randomly divided into six groups and immunized three times during a two-week interval with 100 μL of phosphate-buffered saline (PBS), Omp19, SC-Omp19, SC-Omp19-OPS, AP205-Omp19, or AP205-Omp19-

Table 1
Main plasmids used in this study.

Plasmid	Characteristic	Source
pET-PglL-CTB^{4573C}	Encodes PglL and 6× His-tagged CTB4573, both under control of a Tac promoter; Kan^R	Laboratory stock [16]
pET28a-Omp19	Encodes 6× His-tagged Omp19; Kan^R	This study
pET28a-Omp19G	Encodes glutathione S-transferase (GST)-tagged Omp19; Kan^R	This study
pET28a-SC-Omp19	Encodes 6× His-tagged SC-Omp19; Kan^R	This study
pET28a-PglL-SC-Omp19^{4573C}	Encodes PglL and 6× His-tagged SC-Omp19, both under control of a Tac promoter; Kan^R	This study
pTargetF	Expresses the targeting synthetic guide RNA (sgRNA), Cas9 endonuclease, and arabinose-inducible transcription factor, Spc^R	Laboratory stock [29]
pTargetF-Δ*rfaL*	pTargetF with an N20 sequence for targeting the *rfaL* gene, Spc^R	This study
pCas	Contains the *cas9* gene with a native promoter, an arabinose-inducible sgRNA, the λ-red recombination system, and temperature-sensitive replication, Kan^R	Laboratory stock [29]

OPS. The mice were injected subcutaneously (s.c.) with 20 μg of Omp19 or other proteins containing 20 μg of Omp19, or injected intraperitoneally (i.p.) using a 15 μg dose. The positive control groups were immunized by i.p. injection once with a dose of 1.0×10^6 colony-forming units (CFU) per mouse of *B. melitensis* strain M5-90. The tail-tip blood of mice was taken ten days after each immunization, and the serum was separated and stored at −20 °C. Two weeks after the final immunization, mice were injected i.p. with 1.7×10^7 CFU of M5-90, the mouse weights were recorded, and the bacterial load in the mouse spleens was determined. For a long-term protective evaluation, mice were injected i.p. with 4.0×10^8 CFU of M5-90 14 weeks after the third immunization (18 weeks after the first immunization), and then the mouse survival was monitored.

2.9. Flow cytometry analysis of lymph node cells from immunized mice

Omp19, SC-Omp19-OPS, AP205-Omp19-OPS (all contained 20 μg of Omp19), and a PBS control were injected s.c. into the tail base of BALB/c mice. Some of the treated mice were sacrificed at different time points, and their popliteal dLNs were harvested to prepare single-cell suspensions. At 24 h post injection, the single-cell suspension of dLNs was stained with fluorescein isothiocyanate (FITC)-conjugated anti-mouse CD11c, allophycocyanin (APC)-conjugated anti-mouse CD80, and Alexa Fluor (AF) 700-conjugated anti-mouse major histocompatibility complex (MHC)-II, to analyze the proportion of dendritic cells (DCs) that co-expressed CD80 and MHC-II. On the third day post injection, the single-cell suspension of dLNs was stained with APC-conjugated anti-mouse CD3, FITC-conjugated anti-mouse CD4, and phycoerythrin (PE)-conjugated anti-mouse CD8, to analyze the proportions of $CD4^+$ and $CD8^+$ T cells. On the seventh day post injection, the single-cell suspension of dLNs was stained with APC-conjugated anti-mouse B220 (CD45), Pacific Blue (PB)-conjugated anti-mouse GL-7, and PE-conjugated anti-mouse CD95, to analyze the proportions of germinal center (GC) B cells. The cells were incubated with antibodies for flow cytometry at 4 °C for 30 min, washed three times, resuspended with staining buffer, and analyzed using a CytoFLEX flow cytometer (Beckman Coulter Life Sciences, USA). All the antibodies were from eBioscience (USA).

2.10. Immunofluorescence microscopy of lymph nodes from immunized mice

The BALB/c mice were immunized as described in Section 2.8. Their popliteal dLNs were harvested and fixed with 4% paraformaldehyde on days 7 and 10 post injection. After being washed with PBS, embedded, and sliced into thick sections, the samples were blocked for 30 min with 5% bovine serum albumin, and then stained with Ki67 antibody (Servicebio, China) at 4 °C overnight. After washing with PBS, the samples were further stained with 4′,6-diamidino-2-phenylindole (DAPI) (Servicebio) at room temperature for 30 min and then washed with PBS.

2.11. Safety determination

Six-week-old specific-pathogen-free female BALB/c mice were divided into two groups (n = 5). One group of mice was injected with five times the normal dose of AP205-Omp19-OPS (100 μg Omp19 per mouse), and the other group received no treatment. The body temperatures and weights of the mice were measured at 0, 1, 2, 5, 7, 10, 12, and 14 days after injection. Blood was sampled from the tail vein at 0, 1/2, 1, 2, 7, and 14 days after injection. Then the serum was separated and the cytokine concentrations were determined with mouse tumor necrosis factor-alpha (TNF-α), interleukin-1β (IL-1β), and interleukin-6 (IL-6) precoated enzyme-linked immunosorbent assay (ELISA) kits (Dakewe, China). On day 28 after injection, blood was collected from tail veins and serum levels of alanine aminotransferase (ALT), aspartate transaminase (AST), alkaline phosphatase (ALP), and blood urea nitrogen (BUN) were determined with a Chemray 240 automatic biochemical analyzer (Rayto Life and Analytical Sciences Co., Ltd., China). Mice were sacrificed by cervical dislocation, and the hearts, livers, spleens, lungs, and kidneys were removed and fixed with 4% paraformaldehyde (Solarbio, China). The tissues were embedded and sectioned, then heated in a drying oven, dewaxed, and hydrated. Next, the sections were stained, dehydrated, cleaned for transparency, and sealed with a neutral resin in accordance with the manufacturer's instructions of a hematoxylin and eosin (HE) staining kit (Solarbio).

2.12. ELISA

To exclude the impact of the His tag in the results of the immunizations, we used purified glutathione S-transferase (GST)-tagged Omp19 (GST-Omp19) to coat a 96-well immunoplate for ELISA. Lipopolysaccharide (LPS) extraction was performed as described previously [17,19]. GST-Omp19 (0.1 μg per well) and YeO9_52212 LPS (5 μg per well) were precoated on 96-well immunoplates for 2 h at 37 °C and then washed three times with PBS and 0.05% Tween 20 (PBST). The plates were patted dry and blocked with blocking buffer (PBST + 5% milk powder) at 4 °C overnight. After drying. the plates were incubated with serially diluted serum from the immunized mice at 37 °C for 1 h. The plates were washed three times and dried, then incubated with 1:50 000 diluted HRP-conjugated goat anti-mouse antibody (IgG, IgG1, or IgG2a) (Abcam, China) at 37 °C for 1 h. After another washing and drying step, the color-producing reaction was initiated by using a Soluble TMB Kit (CWBio, China) and terminated with a stop solution (2 $mol \cdot L^{-1}$ H_2SO_4). The absorbance was measured at a wavelength of 450 nm.

2.13. Determination of bacterial load in the spleen and liver after infection

Fourteen days after the third immunization, the mice were injected i.p. with 1.7×10^7 CFU of M5-90 per mouse, A single colony of *B. melitensis* M5-90 was picked and inoculated into TSB medium, and the culture was incubated at 37 °C with 200 revolutions per minute (rpm) shaking to an optical density at 600 nm (OD_{600}) of approximately 2.0 (about 5×10^6 $CFU \cdot \mu L^{-1}$ bacterial fluid). The bacteria were diluted with normal saline according to the needs of the challenge or infection as described below, achieving a final volume of 200 μL per mouse. At the same time, the bacterial culture was diluted to the appropriate concentration with normal saline and dropped on a tryptic soy agar (TSA) plate for counting. The actual bacterial number was determined for challenge or infection. On the sixth day after the non-lethal dose of infection, the mice were killed by cervical dislocation, and the spleen and liver were removed and homogenized with 2 mL of normal saline under sterile conditions. The spleen or liver homogenate was then fully mixed, diluted and cultured on TSA plates. Bacterial colonies were counted after three days of culture at 37 °C.

2.14. Determination of the TNF-α level after infection

Blood was collected on days 0, 3, and 5 from tail veins after mice were infected with a non-lethal dose of M5-90. The serum was separated and TNF-α was quantified with a mouse TNF-α Precoated ELISA Kit (Dakewe).

2.15. Serum bactericidal antibody assay

The sera of each immune group were mixed and incubated at 56 °C for 30 min to inactivate their complement, and then diluted to different concentrations with normal saline. *B. melitensis* strain M5-90 was cultured at 37 °C until the OD_{600} reached approximately 2.0 and then diluted by 1 000 000 times with normal saline. Diluted serum (10 μL), diluted bacterial cells (10 μL), and bovine complement (20 μL) were mixed and incubated at 37 °C for 1 h. Then the mixture was dropped on TSA plates and cultured at 37 °C for 72 h. The number of single colonies was counted to calculate the bactericidal efficiency.

2.16. Statistical analysis

Antibody titers and bacterial loads were lg-transformed. Statistical analyses were conducted using GraphPad Prism version 8.0 (GraphPad, USA). Data were analyzed using the Kruskal–Wallis test or one-way analysis of variance (ANOVA) with Dunn's multiple comparison test. All the data were expressed as means ± standard deviations (SDs). Values of $p < 0.05$ were considered statistically significant ($^{****}p < 0.0001$, $^{***}p < 0.001$, $^{**}p < 0.01$, and $^{*}p < 0.05$).

3. Results

3.1. Design and production of a dual-antigen nanoconjugate vaccine

YeO9, has an OPS repeat unit which is the same as that of *B. abortus* and that is also the main component of OPS in *B. melitensis* (Fig. S1 in Appendix A). Our previous study showed that conjugate vaccine C-OPS_{Ba} could protect mice from the lethal challenge of *B. abortus* [19]. However, subsequent results indicated a limited effect of this conjugate vaccine against *B. melitensis*, the most prevalent *Brucella* strain in humans, which has a similar yet slightly different structure of the polysaccharide antigen [7,30]. Thus, to prepare a more efficient *Brucella* vaccine, we developed a novel strategy for producing a high performance nanoconjugate vaccine, containing two different type of antigens and loaded on AP205, a widely reported efficient nano-carrier (Fig. 1(a)). We first optimized the host bacteria YeO9_52212 by knocking out the O-antigen ligase gene *rfaL* (Fig. S2 in Appendix A) that controls the transfer of OPS to the lipid A core, resulting in more OPS linked to the undecaprenol pyrophosphate, which is the substrate for PglL. As expected, by introducing the glycosylation system, we found that more OPS coupled to carrier proteins in the gene deletion strain YeO9_52212Δ*rfaL* (Fig. S3 in Appendix A). Then, to produce a dual-antigen module, containing both the polysaccharide (OPS) and protein antigen (Omp19), we constructed a vector pET28a-PglL-SC-$Omp19^{4573C}$, which co-expressed PglL and a fusion protein of SC, antigen Omp19, the glycosylation sequence 4573, and a 6× His tag. After being introduced into YeO9_52212Δ*rfaL* and induced with IPTG, SC-Omp19-4573-His tag was expressed and OPS was loaded via the catalysis of PglL *in vivo*. The final product, SC-Omp19-OPS, was then purified by affinity and SEC (Fig. S4 in Appendix A).

Given the fact that ST and SC could form a spontaneous isopeptide bond *in vitro*, we used an ST-AP205 [21] to realize a covalent connection between the antigens and nanoparticle. To determine the optimal combination ratio of SC-Omp19-OPS and ST-AP205, the purified ST-AP205 and SC-Omp19-OPS were mixed at different molar ratios. After incubating at 4 °C overnight, SDS-PAGE was performed and the results showed that a saturated reaction of ST-AP205 required a 4-fold molar excess of SC-Omp19-OPS, as no additional conjugated products were generated after adding more SC-Omp19-OPS (Fig. 1(b)). To remove the uncoupled SC-Omp19-OPS, the mixture was further purified by SEC and the target protein was eluted in about 65 mL from a column with a 200 mL column volume (Fig. 1(c) and Fig. S5 in Appendix A), ensuring that there was no free SC-Omp19-OPS in the final product (AP205-Omp19-OPS). Then, AP205-Omp19-OPS was confirmed by SDS-PAGE and Western blotting analysis using anti-His antibody and anti-YeO9 serum, and an obvious shift in the molecular weight of SC-Omp19-OPS (from 35 to 50 kDa) was observed (Fig. 1(d)). Subsequent transmission electron microscopy (TEM) images of AP205-Omp19-OPS showed non-aggregated spherical particles, with a size of about 50 nm in diameter (Fig. 1(e)). DLS analyses revealed that AP205-Omp19-OPS had a homogeneous size distribution; these findings were in line with the TEM results (Fig. 1(f)). Then, to evaluate the stability of the nano conjugate vaccine, the AP205-Omp19-OPS solution was held at room temperature for at least 72 h, and the particle size was consistent at different time points (Fig. 1(g)). Furthermore, there was no obvious size change when the solution was lyophilized and reconstituted, as determined by DLS analysis, indicating good stability of the nanoconjugate vaccine (Fig. 1(h)).

3.2. The nanoconjugate vaccine elicits an effective immune activation

To determine the immune activation ability of the dual-antigen nanoconjugate vaccine, AP205-Omp19-OPS, and the other control vaccines, including Omp19 (Figs. S6 and S7 in Appendix A), SC-Omp19-OPS, and PBS, were injected into the tail base of BALB/c mice. At 24 h post injection, some of the treated mice were sacrificed and their dLNs were extracted for flow cytometry. The results showed that the DCs expressing the co-stimulatory marker CD80 and T cell recognition signal MHC-II in the dLN of mice immunized with AP205-Omp19-OPS was significantly higher than those of the other groups (Fig. 2(a)). In addition, the proportion of $CD80^+$ $MHC\text{-}I^+$ DCs also increased significantly in AP205-Omp19-OPS-treated mice (Fig. S8 in Appendix A), indicating that the nanovaccine had the highest activation of DCs and was better presented compared to the other vaccines. On the third day after immunization, we further examined the distribution of T cells in the lymph nodes. We found that the number of T cells in the Ap205-Omp19-OPS-treated dLNs was much higher than that in the other groups, and resulted in an obvious enlargement of the dLNs (Fig. 2(b)), which was primarily due to the proliferation of T cells. Furthermore, by analyzing the T cell subtypes, we found that the distribution of both $CD4^+$ and $CD8^+$ T cells were in line with the results of the total T cells (Fig. 2(c)), suggesting that both humoral immunity and cellular immunity were activated. Given that the activation of GCs determines the production of antibodies, we next evaluated the proliferation of B cells in the GC on day 7 post injection. The results of flow cytometry showed that the proportions of GC B cells were higher in the AP205-Omp19-OPS vaccinated group compared with the other groups (Fig. 2(d)). The number of GCs was dramatically increased in the dLNs of AP205-Omp19-OPS immunized mice, according to the immunofluorescence staining for the proliferative marker Ki67 on days 7 (Fig. 2(e)) and 10 (Fig. S9 in Appendix A). Thus, the nanovaccine greatly promoted the immune response.

3.3. The dual-antigen nanoconjugate vaccine is safe in vivo

After confirming the highly efficient immunostimulatory capacity of the dual-antigen nanoconjugate vaccine, we then further evaluated the safety of the vaccine before mouse immunization experiments. Briefly, BALB/c mice were injected with AP205-Omp19-OPS (containing 100 μg of Omp19, five times the normal immune dose) and then a series of safety indicators were monitored at different time points (Fig. 3(a)). During the

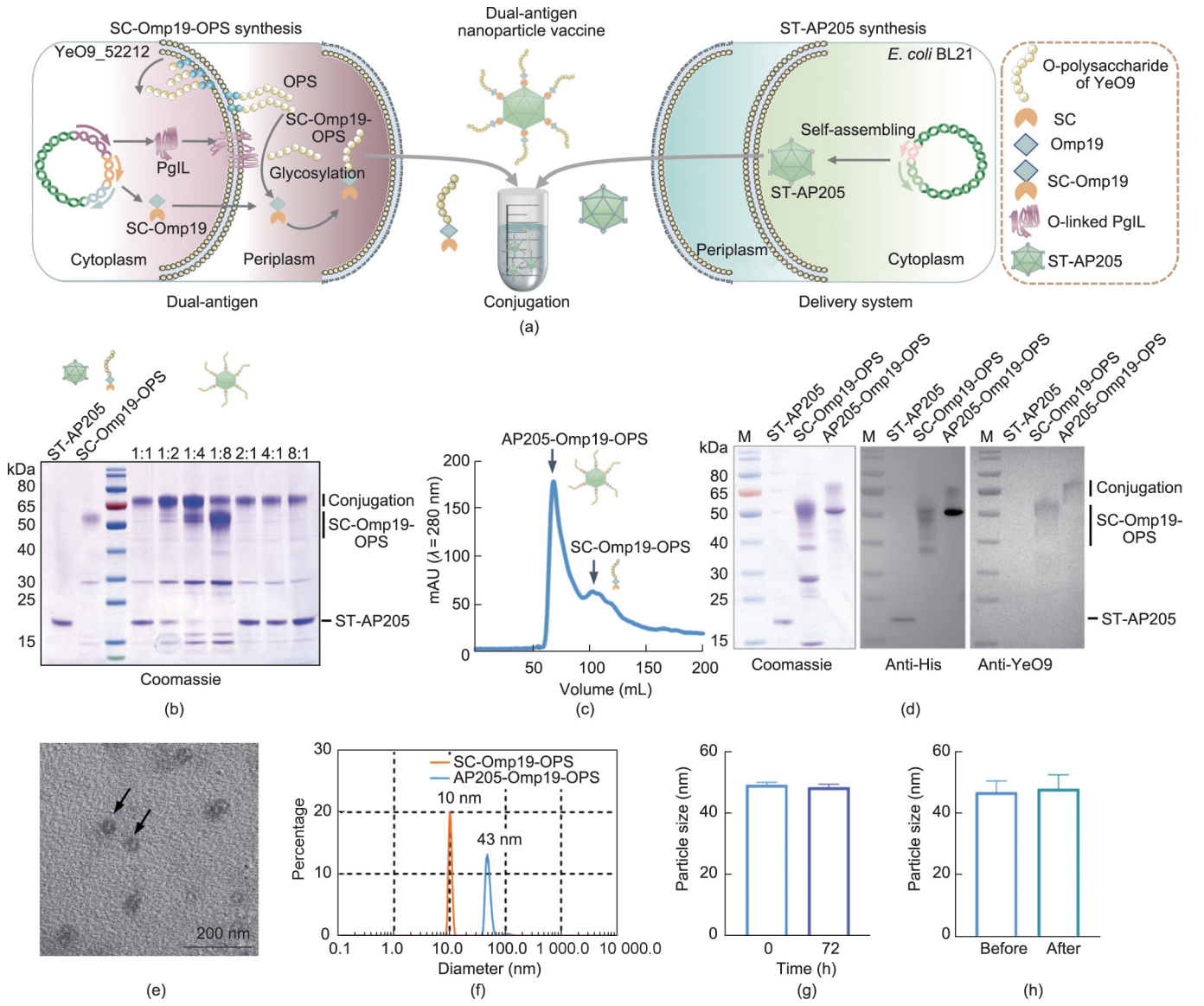

Fig. 1. Construction and characterization of the dual-antigen nanoconjugated vaccine. (a) Schematic diagram of the dual-antigen nanoconjugated vaccine production. (b) Coupling of the dual-antigen SC-Omp19-OPS and delivery system ST-AP205 at different molar ratios, and analysis by Coomassie blue staining. (c) SEC of the mixture of ST-AP205 and SC-Omp19-OPS at the optimum molar ratio, with different glycoprotein peaks indicated by black arrows. (d) Purified ST-AP205, SC-Omp19-OPS, and AP205-Omp19-OPS analyzed by Coomassie blue staining, Western blotting analysis using anti-6× His tag (anti-His) antibody, and anti-YeO9-specific monoclonal antibody. (e) TEM image and (f) DLS analysis of AP205-Omp19-OPS. (g) DLS analysis of AP205-Omp19-OPS particle size before and after the particles were stored at room temperature for 72 h. (h) DLS analysis of AP205-Omp19-OPS particle size before and after lyophilization and reconstitution. M: marker.

observation period, the vaccinated mice showed no signs of anomaly, such as body weight loss or temperature changes (Fig. 3(b)). Then, three major inflammatory factors, including TNF-α, IL-1β, and IL-6, were measured in the serum of each mouse at different time points. We found that all indicators remained at a very low level (Fig. 3(c)), suggesting that the nanoconjugate vaccine induced almost no inflammatory response. Furthermore, histological analysis of the organs, including heart, liver, spleen, lung, and kidney, were performed 14 days after administration. As expected, no damage or pathological alterations were detected in the tissue sections (Fig. 3(d)). In addition, we also determined biochemical indices, include ALT, ALP, AST, and BUN, in the serum on the 28th day post vaccination, and all the biomarkers in both immunized and normal (untreated) mice were within the normal range (Fig. 3(e)). These above results showed that the nanovaccine was safe and appropriate to use in further evaluations.

3.4. Immune effect of dual-antigen nanoconjugate vaccine via s.c. injection

Encouraged by the pronounced immune activation ability and safety of the dual-antigen nanoconjugate vaccine, we further evaluated the vaccine effect through a series of mouse experiments. The BALB/c mice were injected s.c. with Omp19, SC-Omp19, SC-Omp19-OPS, AP205-Omp19, or AP205-Omp19-OPS (each injection contained 20 μg of Omp19) at 0, 14, and 28 days (Fig. S7), and PBS was used as the control (Fig. 4(a)). Blood was collected on day 38 from tail snip of each mouse to measure the specific serum antibody against Omp19 and OPS. The ELISA results showed that the Omp19-specific IgG titers were observed in all of the Omp19-treated groups, and AP205-Omp19-OPS elicited the most robust antibody response compared with the others, and was increased over 1000-fold compared with

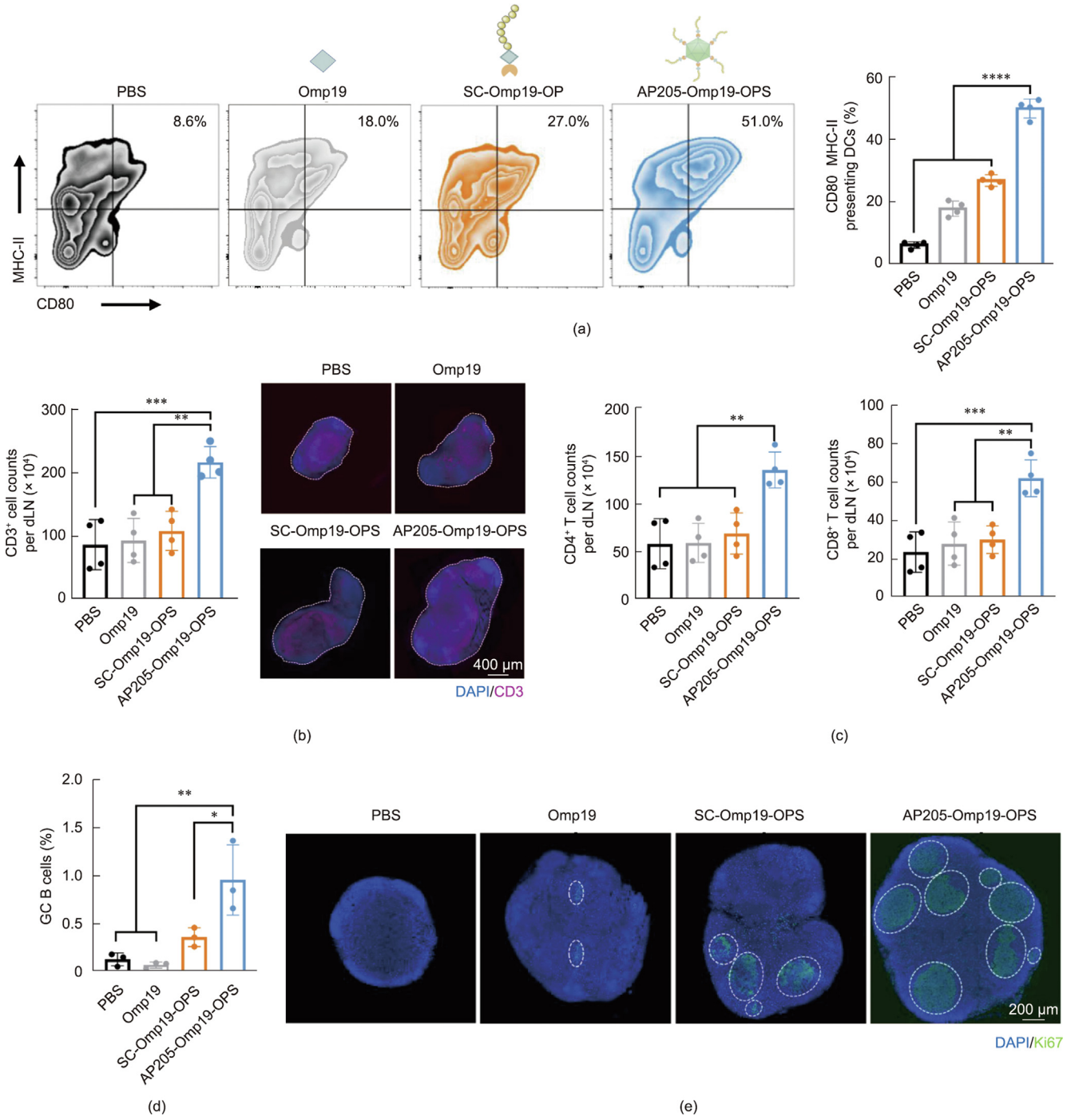

Fig. 2. The nanoconjugated vaccine effectively activated an immune response. BALB/c mice were immunized s.c. with PBS, Omp19, SC-Omp19-OPS, or AP205-Omp19-OPS, and dLNs of mice were collected at 24 h after injection and analyzed by flow cytometry for (a) the proportion of DCs that co-expressed CD80 and MHC-II (n = 4). On the third day, lymph nodes were extracted from mice for immunofluorescence analysis and stained with DAPI (blue) and CD3 (pink), and examined for (b) the number of $CD3^+$ cells, and (c) $CD4^+$ T and $CD8^+$ T cells among total dLN cells (n = 4). On the seventh day post injection, lymph nodes were collected and analyzed for (d) the proportion of GC B cells (n = 3) and (e) immunofluorescence staining of dLNs (blue: DAPI; green: Ki67), with the distribution of GCs shown by white dashed lines. Data are presented as the means ± SD and analyzed by one-way ANOVA with Dunn's multiple comparison test. $^{****}p < 0.0001$, $^{***}p < 0.001$, $^{**}p < 0.01$, and $^{*}p < 0.05$.

Omp19 alone (Fig. 4(b) and Fig. S10 in Appendix A). By further analyzing the IgG subtype, we found that both IgG1 and IgG2a in AP205-Omp19-OPS-immunized mice were greatly increased (Fig. 4(c) and Fig. S11 in Appendix A), indicating that both humoral and cellular immunity responses were enhanced when antigens were loaded in the nanoparticle. The IgG titers and two subtypes (IgG1 and IgG2a) against YeO9_52212 LPS were also increased in the AP205-Omp19-OPS group, which was consistent with the results for Omp19 (Figs. 4(d) and (e)). Given that the titer ratios of IgG1/IgG2a are commonly used as an indicator of potential Th1 or Th2 responses, we further calculated the titers ratios of different IgG subtypes and found that a mixed and balanced IgG1/IgG2a systemic response (the ratio of IgG1/IgG2a was about 1.0) [31] was evoked by the dual-antigen nanovaccine, indicating evidence of both Th1 and Th2 activation (Figs. 4(c) and (e)). Taken together, these results showed that AP205-Omp19-OPS efficiently produced specific antibodies against both Omp19 and OPS antigens.

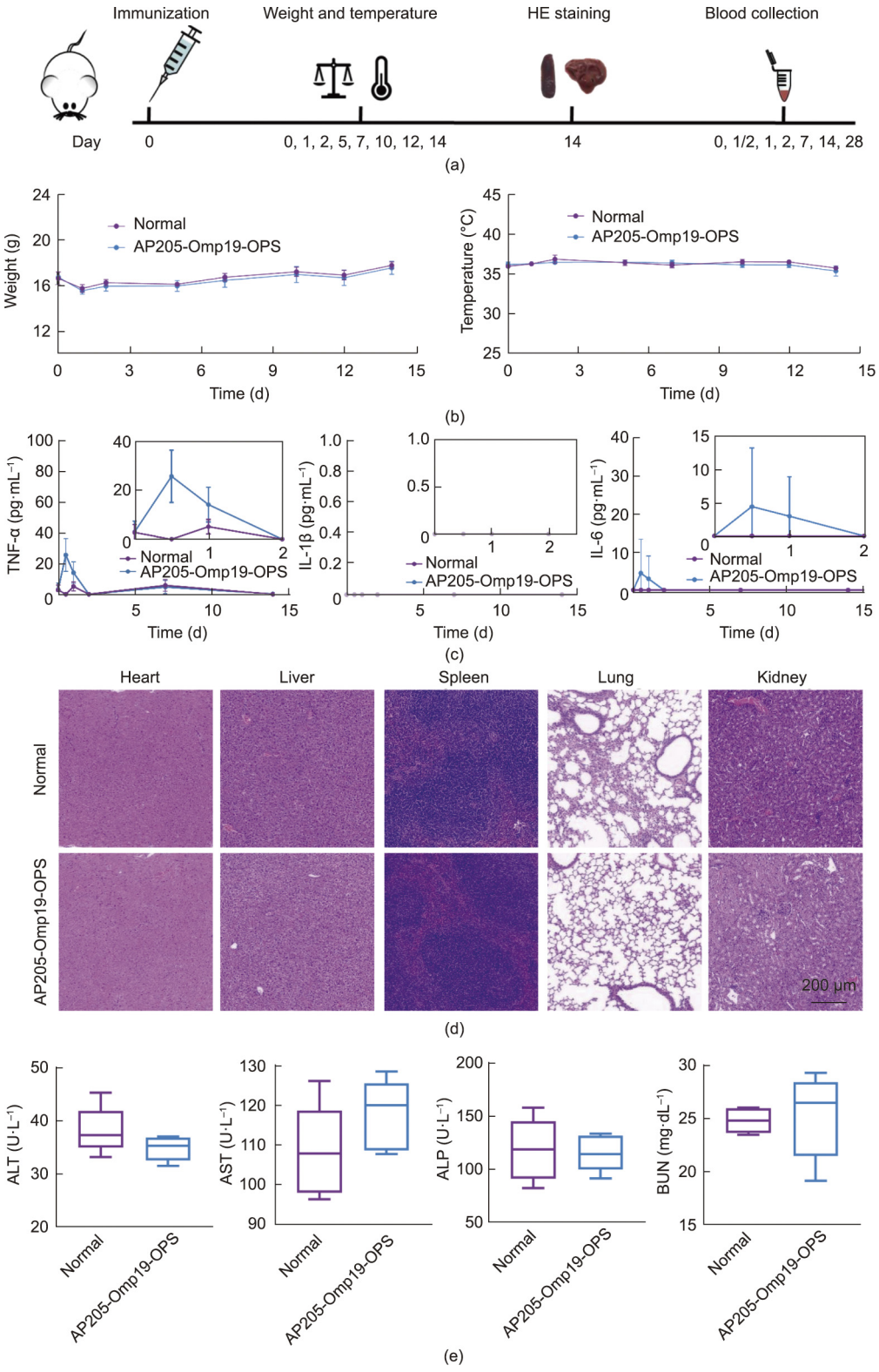

Fig. 3. Safety evaluation of the dual-antigen nanoconjugate vaccine. (a) Experimental schedule for the safety evaluation of nanoconjugate vaccine. (b) Body weight and rectal temperature changes in mice treated once with AP205-Omp19-OPS and normal (untreated) mice. (c) Serum cytokine levels (TNF-α, IL-1β, and IL-6) at different time points post immunization. (d) Histological analysis of heart, liver, spleen, lung, and kidney of treated mice on the 14th day after treatment and of normal mice. (e) The levels of ALT, ALP, AST, and BUN in the serum of treated mice on the 28th day after immunization and in normal mice.

Then, the protective effect of the candidate nanovaccine was evaluated through non-lethal infections of *B. melitensis*. Each immunized mouse received *B. melitensis* M5-90 at a dose of 1.7×10^7 CFU via i.p. injection 14 days after the third immunization. Although body weight in all the M5-90-infected mice quickly reduced compared with normal mice, the weight of mice

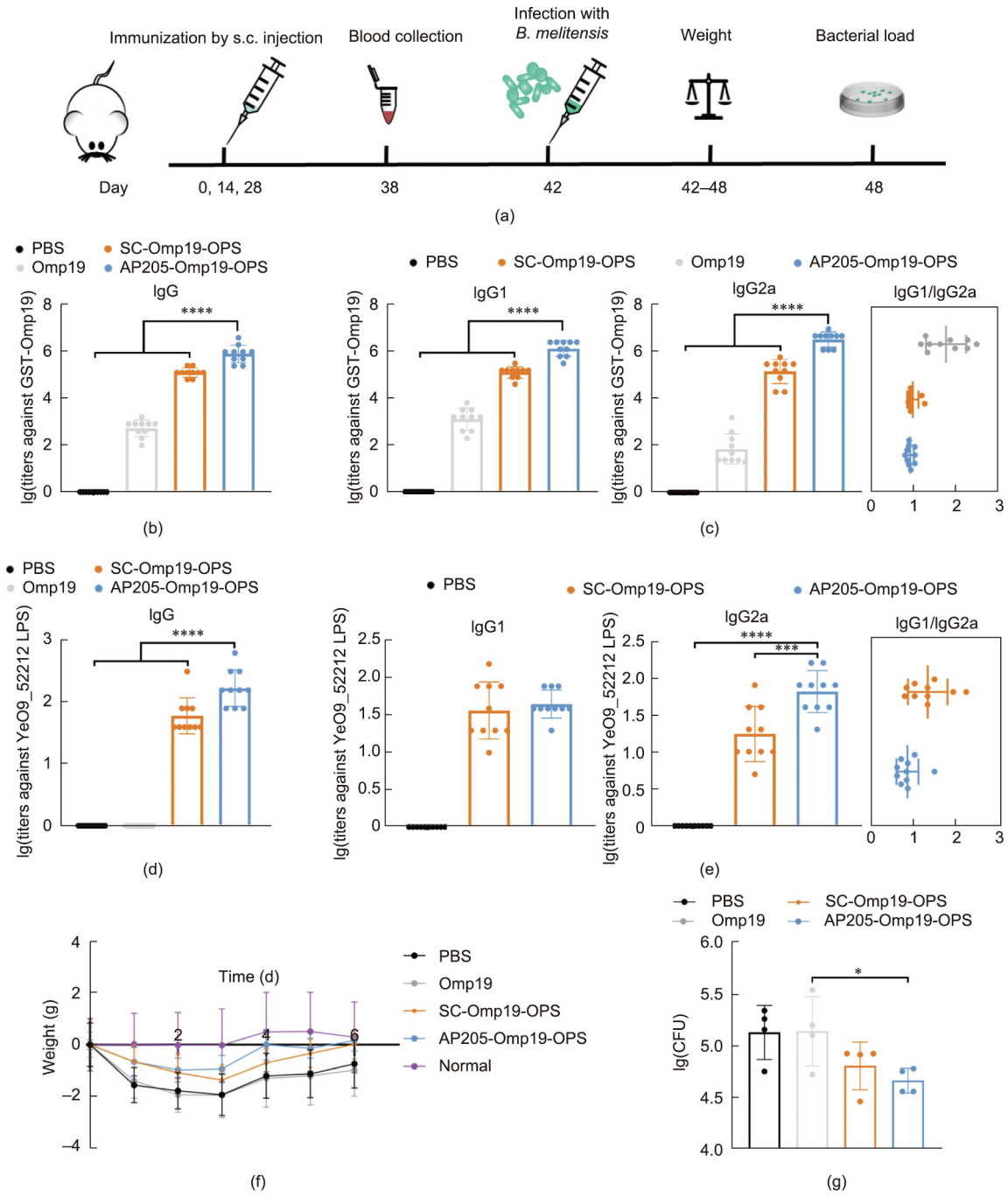

Fig. 4. Evaluation of humoral immunity and protection against non-lethal *B. melitensis* M5-90 infection elicited by s.c. injection of dual-antigen nanoconjugate vaccine. (a) Schematic diagram of the s.c. injection study. The serum (b) IgG, and (c) IgG1 and IgG2a responses against GST-Omp19 after the third s.c. injection. The 96-well plates were coated with purified GST-Omp19 (n = 10). The serum (d) IgG, and (e) IgG1 and IgG2a responses against LPS of YeO9_52212 after third s.c. injection. The 96-well plates were coated with LPS of YeO9_52212 (n = 10). (f) Weight change of immunized mice after infection with M5-90 (n = 5). (g) Bacterial load in the spleen of mice after infection with non-lethal *B. melitensis* M5-90 (n = 4). Data are presented as means ± SD and analyzed by one-way ANOVA with Dunn's multiple comparison test. $^{****}p < 0.0001$, $^{***}p < 0.001$, and $^{*}p < 0.05$.

in the AP205-Omp19-OPS group showed the least reduction and fastest recovery (Fig. 4(f) and Fig. S12 in Appendix A). Then the mice were sacrificed six days after infection and the bacterial load in spleens and livers was quantitated. The results showed that the number of bacteria in both organs was lower in AP205-Omp19-OPS-immunized mice than in the others, and was particularly significant in the livers (Fig. 4(g) and Fig. S13 in Appendix A), indicating that AP205-Omp19-OPS elicited better protection against non-lethal infection of *B. melitensis* compared with Omp19.

3.5. Immune effect of dual-antigen nanoconjugate vaccine via i.p. injection

Once we had confirmed the immune enhancement and protective effects of the nanovaccine through the s.c. route, we evaluated its effects via the i.p. route, another commonly used vaccination method. Mice were immunized i.p. with PBS, Omp19, SC-Omp19, SC-Omp19-OPS, AP205-Omp19, or AP205-Omp19-OPS on days 0, 14, and 28, and a separate positive group were injected i.p. with 1.0×10^6 CFU of *B. melitensis* M5-90 per mouse. Except for the

PBS and M5-90 groups, all groups were immunized with 15 μg of Omp19. In addition to determining the induced antibody titer of each group, a series of protective indicators were evaluated after infection with a non-lethal dose of *B. melitensis* (1.7×10^7 CFU per mouse) on day 42 (Fig. 5(a)). Similar to the results from the s.c. route, the specific IgG titers against Omp19 were significantly increased in both the SC-Omp19-OPS and AP205-Omp19-OPS groups, with the increases were most profound for the AP205-Omp19-OPS-treated mice (Fig. 5(b) and Fig. S14 in Appendix A). In the AP205-Omp19-OPS group, both IgG1 and IgG2a titers were significantly higher than in the other groups (Fig. 5(c) and Fig. S15 in Appendix A). The same trend was also found in serum antibody responses against OPS. AP205-Omp19-OPS induced remarkably higher IgG and other antibody subtypes against YeO9_52212 LPS compared with SC-Omp19-OPS (Figs. 5(d) and (e)).

Next, we evaluate the protection of each treatment after infection of *B. melitensis* M5-90 with a non-lethal dose as described above. The weight loss of the AP205-Omp19-OPS group was the least, suggesting that this group had better protection against infection-associated weight loss than the other groups, especially when compared to the positive control M5-90 group (Fig. 5(f) and Fig. S16 in Appendix A). Given that the secretion of TNF-α is highly associated with the inflammatory responses caused by *B. abortus* infection [19], we then measured the concentration of TNF-α in the serum from each mouse at days 0, 3, and 5 post-infection with M5-90 (days 42, 45, and 47 post first immunization). The results showed that although TNF-α levels in all groups increased following infection, only a very low concentration (less than 11 $pg \cdot mL^{-1}$) was found in mice immunized with AP205-Omp19-OPS, indicating almost no systemic inflammatory reaction in this group (Fig. 5(g) and Fig. S17 in Appendix A).

We next examined the bacterial load in the spleens of immunized mice. The results showed that the AP205-Omp19-OPS group (with a protection unit of 1.22) had the lowest colony number compared with the Omp19 and SC-Omp19-OPS groups (Fig. 5(h) and Fig. S18 in Appendix A). Moreover, histological analyses of spleens and livers of the M5-90-infected mice showed that, similar to the positive control group M5-90, immunization of AP205-Omp19-OPS largely alleviated desmoplasia and multinucleated giant cell proliferation in the spleens, and decreased inflammatory cell infiltration in livers, which also supported these results (Fig. 5(i) and Fig. S19 in Appendix A). These results further confirmed that the nanovaccine AP205-Omp19-OPS engendered strong protective effects against *B. melitensis*.

3.6. Long-term protective effect of the dual-antigen nanoconjugate vaccine

Because an ideal vaccine for use in humans or in animals should be effective and avirulent, and induce long-lasting protection [32], we further evaluated the long-term protection of this dual-antigen nanoconjugate vaccine. The mice were grouped and immunized as described previously and blood samples of each mouse were collected at each time point for subsequent tests. Eighteen weeks after the first immunization, the mice were challenged with a lethal dose of *B. melitensis* M5-90 strain (Fig. 6(a)). During the monitoring period, the peaks of the antibody titer against Omp19 of each immunized group appeared in the 10th week, and the titer in the AP205-Omp19-OPS group remained the highest for at least 18 weeks (Fig. 6(b) and Fig. S20 in Appendix A). Then, by detecting serum subtypes, we found that IgG1 and IgG2a serum titers of the AP205-Omp19-OPS-immunized group showed no difference 6 and 18 weeks after the first immunization (10 days after the last immunization) (Fig. 6(c)). For OPS, the IgG titer in the AP205-Omp19-OPS group showed almost no reduction, while in the SC-Omp19-OPS group, it gradually decreased from the 10th week (Fig. 6(d)). Furthermore, the OPS-specific IgG1 and IgG2a titers at the end time point were even higher than that at the sixth week (Fig. 6(e)). These results indicated that the dual-antigen nanoconjugate vaccine elicited a potent and stable long-term immune response against both types of antigens. Moreover, we performed the bactericidal assays and found that although serum collected at six weeks from the Omp19 and SC-Omp19-OPS groups showed little bactericidal activity, AP205-Omp19-OPS-immunized serum reduced the viability of *B. melitensis* M5-90, and the bactericidal activity was maintained until the 18th week (Fig. 6(f)). Additionally, mice from each treatment group were inoculated i.p. with approximately 4.0×10^8 CFU per mouse (about 5× lethal dose) of the M5-90 strain 18 weeks post immunization and mouse survival was monitored. With this strong pathogen challenge dose, almost all of the mice from the PBS, Omp19, SC-Omp19, SC-Omp19-OPS, and AP205-Omp19 groups were dead within three days. The positive control M5-90 group only had a 20% protection, while 60% of the AP205-Omp19-OPS-treated mice survived, which was higher than the survival of the positive control (Fig. 6(g)). This result indicated that the nanoconjugate vaccine efficiently protected mice from the infection of *B. melitensis* for at least three months.

4. Discussion and conclusion

It has been widely demonstrated that vaccines with broad-spectrum protective effects can be produced by combining multiple antigen components into a single vaccine [33,34]. The use of multivalent vaccines should allow better coverage of natural pathogen antigen diversity, better match the genetic variability of the human immune system, and reduce the risk of pathogen escape due to immune pressure [35]. However, a simple mixture of different antigens does not assure delivery of the target peptide epitopes, T-helper epitopes, and adjuvants to the same antigen-presenting cells, and therefore may impair immune responses [35]. In contrast, a covalently bound combination of various antigens would ensure co-delivery of the vaccine components. Different from other multiple-antigen vaccines, here, the polysaccharide and protein antigens were simultaneously loaded on a single nano-carrier. In our design, we used the O-linked glycosylation system to generate a dual antigen module. Because Omp19 contains a glycosylation sequence, OPS can be coupled to it through the catalysis of PglL in *Y. enterocolitica*. By a similar approach, the OPS could be coupled with other protein antigens (e.g., Omp31, L7/L12, and lumazine synthase) or multiple-protein fusion antigens in the future to prepare more efficient *Brucella* vaccines. In addition, the accelerating development and application of bioinformatics techniques have given rise to a new field of vaccine design, in which vaccine protein candidates are predicted *in silico* from genome sequences using reverse vaccinology [36,37]. Chimeric proteins based on B and T cell epitopes could also be used to replace Omp19 to increase the possibility of eliciting a broad cellular or humoral immune response [38]. Thus, we provide an evolvable vaccine preparation strategy to prepare broad-spectrum vaccines.

Many types of anti-*Brucella* vaccines have been developed, mainly including live attenuated vaccines, DNA vaccines, and subunit vaccines. The live attenuated vaccines have good efficacy but are only licensed for use in livestock due to safety concerns [9,39]. DNA vaccines can induce strong Th1 immune responses and activate cytotoxic T lymphocytes, but fail to provide long-term protection due to the rapid silencing of DNA, thus requiring repeated booster dosing and adjuvants [39]. Subunit vaccines might be the best choice for developing a vaccine for human use. However, most of the reported subunit vaccine candidates

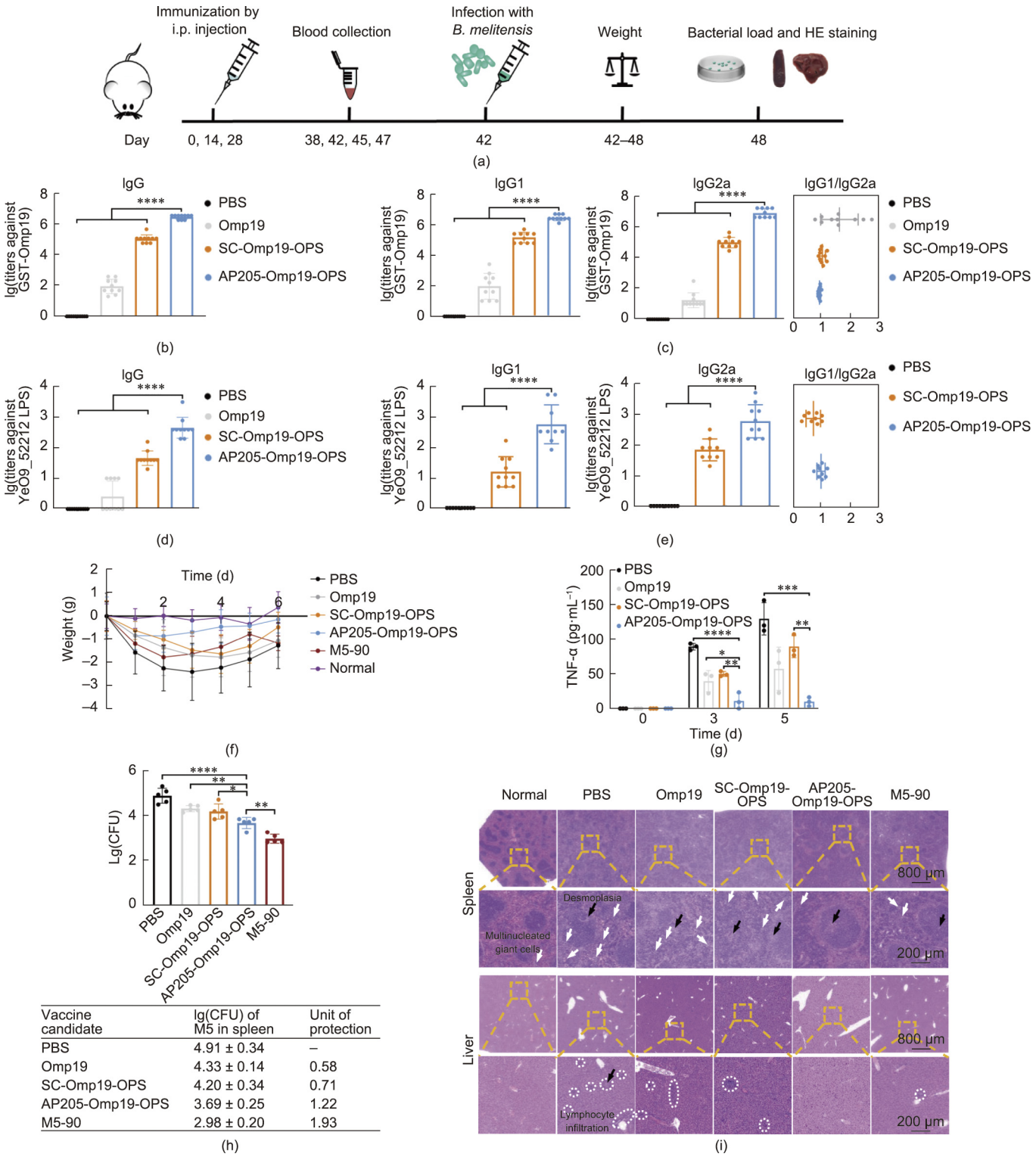

Fig. 5. Evaluation of humoral immunity and protection against non-lethal *B. melitensis* M5-90 infection elicited by i.p. injection of the dual-antigen nanoconjugate vaccine. (a) Schematic diagram of the animal i.p. injection procedure. The serum (b) IgG, and (c) IgG1 and IgG2a titers against GST-Omp19 were measured in immunized groups on day 10 after the third i.p. injection (n = 10). The serum (d) IgG, and (e) IgG1 and IgG2a titers against the LPS of YeO9_52212 were measured in immunized groups on day 10 after the third i.p. injection (n = 10). (f) Weight change of mice treated with different vaccine candidates after infection with M5-90 (n = 5). (g) TNF-α levels in the serum of mice after infection with M5-90 (n = 3). (h) Quantification of bacterial colonization in spleens collected from immunized mice at the sixth day post challenge (n = 5). The splenic bacterial load of the mice was determined and expressed quantitatively in the upper graph in the lower table. (i) Histological analysis of the spleen and liver of infected mice and normal mice. On the sixth day after infection with M5-90, the mice were killed by cervical dislocation, and then the spleen and liver were dissected to observe the pathological changes. The yellow dotted boxes in the top panels represent the field of view in the corresponding figures below, and the scale bars are at the bottom of the figure. Black arrows indicate desmoplasia, white arrows indicate multinucleated giant cells, and white dotted circles indicate lymphocyte infiltration. Data are presented as means ± SD and analyzed by one-way ANOVA with Dunn's multiple comparison test. $^{****}p < 0.0001$, $^{***}p < 0.001$, and $^{**}p < 0.01$, and $^{*}p < 0.05$.

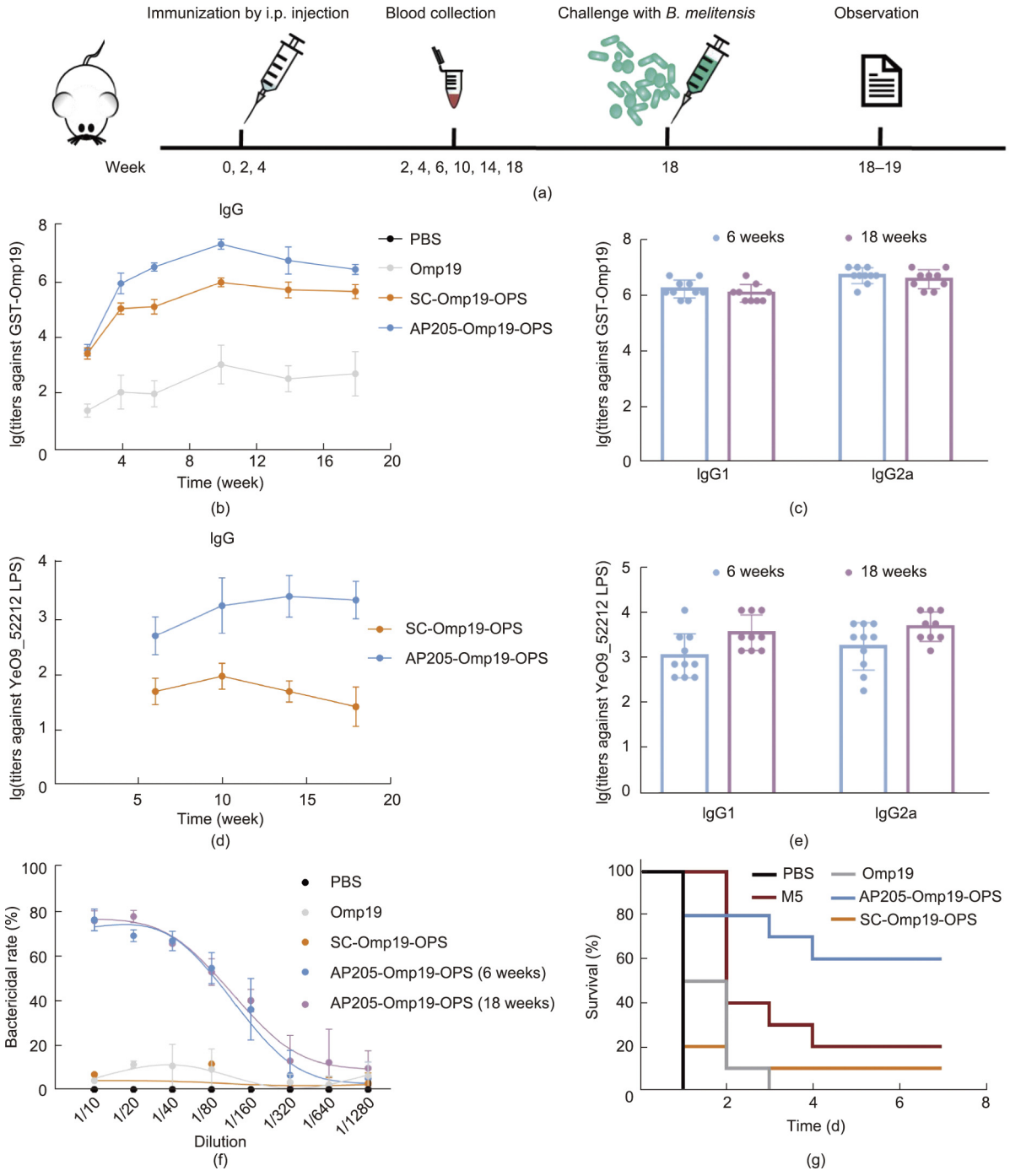

Fig. 6. Evaluation of long-term antibody response and protection against a lethal dose of *B. melitensis* M5-90. (a) i.p. treatment and evaluation schedule for long-term protection. (b) Long-term IgG titers against GST-Omp19 from each treated group were measured over time (n = 10). (c) Serum IgG1 and IgG2a titers against GST-Omp19 of AP205-Omp19-OPS-treated mice 6 and 18 weeks after the first immunization (n = 10). (d) Long-term IgG titers against YeO9_52212 LPS from each treated group (n = 10). (e) Serum IgG1 and IgG2a titers against YeO9_52212LPS of the AP205-Omp19-OPS-treated mice 6 and 18 weeks after the first immunization (n = 10). (f) Serum bactericidal activity of serum from each group 6 weeks after the first immunization, and the serum of the AP205-Omp19-OPS-treated group 18 weeks after the first immunization (n = 3). (g) Survival rates of different groups of mice after challenge with a high dose of *B. melitensis* strain M5-90 (4.0×10^8 CFU per mouse) 18 weeks after the primary immunization (n = 10).

against *Brucella* did not reach the protection efficacy achieved by live attenuated vaccines [10,39]. This was mainly due to the insufficient immunogenicity of the currently identified *Brucella* protein antigens. In our design, the surface-exposed antigenic polysaccharide and outer membrane protein were biosynthesized simultaneously as a unique glycosylated protein. Proteinaceous nanoparticle AP205 was further designed as a "plug and display" carrier to realize the co-delivery of two types of antigens [40]. Moreover, the efficacy of this nanovaccine was good even without the help of adjuvants. Thus, we believe that this work extends subunit vaccine design strategies and will be applicable to the development of nanovaccines against bacterial infections.

A cell-mediated immune response is required to prevent infection of intracellular bacteria such as *Brucella*. In our results, we confirmed that the dual-antigen nanoconjugate vaccine promoted $CD8^+$ T cell differentiation (Fig. 2(c)) and promoted Th1 immune

responses, indicating that cellular immunity was also induced. To further enhance this response, many strategies could be applied. Because the dual-antigen nanoconjugate vaccine was produced based on a modular and flexible strategy, the protein antigen could be easily replaced to improve the cellular immune response. A series of highly effective protein antigens or peptide epitopes can be used. For example, many potential antigenic epitopes of *Brucella* were discovered by screening the MHC-I binding peptides, which could be recognized to promote cross presentation [41,42]. In addition, novel efficient adjuvants (such as IL-18, glycoprotein 96 (gp96), and cytosine-guanine dinucleotide sequence (CpG)) [43–45] have been developed that show pronounced abilities to induce the cellular immune response. These adjuvants are expected to further promote cellular immune responses. Notably, CpG 1018 is currently under evaluation in clinical trials for coronavirus disease 2019 (COVID-19) vaccines [45].

Given that nano-carriers can display antigens at a high density and greatly activate immune responses [46], we chose to use VLPs, the nanoparticles currently approved for vaccines for human use, to load antigens [20]. Although antigens could be coupled on particles through genetic fusion expression or chemical conjugation [21], these methods inevitably affect the structure of the antigen or nano-carrier [22,23]. Therefore, we used the ST/SC system to connect the dual-antigen and AP205 nanoparticle *in vitro*, to ensure the structural integrity as well as the correct assembly of the antigen and nanoparticle. Furthermore, compared with other types of delivery materials, this proteinaceous nanoparticle has higher safety and biological compatibility, which is more conducive to the development of prophylactic vaccines. As expected, our results showed no drug-related toxicity signs in mice after the injection of the vaccine at five times the normal dose.

In order to evaluate the effect of the nanovaccine more comprehensively, two of the most commonly used immunization routes (s.c. and i.p.) were used. We found that both routes induced high levels of antibody responses and provided protection in mice. Cellular immunity is very important for the elimination of intracellular bacteria in the body [8]. Our results showed that the nanovaccine enhanced Th1 and Th2 immune responses at the same time, whether through s.c. or i.p. routes. Th1-associated antibodies were found to enhance the ability of complement killing and opsonization, which may also have an important role in reducing the bacterial load before the organism becomes intracellular [47,48]. Interesting, we detected distinct bactericidal activity against the *B. melitensis* M5-90 strain from the dual-antigen nanoconjugate vaccine immunized mice serum, which was not reported in other studies on *Brucella* vaccines. This finding suggested that the ability of complement-mediated killing by immunized serum is probably important for *Brucella* clearance and could be used as an indicator to evaluate the protective effect of the *Brucella* vaccine. It also should be mentioned that, even with the same vaccine, the reaction quality and the protective effects were shown to be different through various administration routes [49,50]. This view is consistent with our results, in which i.p. immunization elicited higher antibody titers and provided better pathogen clearance than the s.c. route. Moreover, other studies have shown that oral or mucosal immunization of *Brucella* vaccines can also achieve good immune effects [8,51]. Inspired by this point, we will further optimize the route of administration and immunization procedures to achieve the most effective vaccination effect.

Taken together, we have established a safe and effective vaccine candidate against *B. melitensis*, which causes significant animal and human health impacts. In this study, the number of animals used in flow cytometry and for the cytokine assay was limited ($n < 5$); however, this has been commonly accepted in many previously published articles [52–54]. We believe that the use of a larger number of animals in future research will help to further confirm our conclusions. The vaccine in its current stage is not appropriate for animal use, mainly because of the high cost. In the future, we will optimize the entire production process (especially screening for high-yielding host strains) to reduce the total costs, and we believe that after breaking the shackles of the production process, this vaccine will be used in both animals and humans. In our research, we introduced an innovative protein glycosylation system to realize simultaneous loading of polysaccharides and protein antigens on the nanoparticle. This nanoconjugate vaccine caused a remarkable immune response and provided efficient protection. In particular, the long-term protection was better than the attenuated live vaccine strain M5-90. To our knowledge, this is the first attempt to deliver more than one antigen simultaneously through a nano delivery system to protect against infection from *Brucella*, rather than a simple physical mixing of antigens. It should be emphasized that what we provide is a modular antigen preparation technology, which can simultaneously load polysaccharides and various protein antigens. In addition to the Omp19 used in this study, other efficient proteins or multi-epitope peptides can also be co-delivered with polysaccharide antigens. Moreover, our strategy could also be applied to other delivery systems (e.g., other VLPs and ferritin particles) to load additional polysaccharide antigens, making it more conducive to develop bacterial vaccines, such as *Vibrio cholerae* and *Burkholderia pseudomallei*, for which subunit vaccine targeting one antigen is very difficult to achieve satisfactory results [55,56].

Considering that our bioconjugate nanovaccines are based on a proteinaceous scaffold and can provide a better protective efficacy even without adjuvants, many potential studies can be envisioned and conducted in the future. For example, multivalent vaccines could be designed to provide broader protection. As is known, a single antigen generally cannot provide comprehensive protection against certain pathogen genera. Many studies have confirmed that multiple antigens, especially different types of antigens, can provide better immune effects against various clinically isolated pathogens [57–59]. In addition to the ST/SC system we used here, other bioorthogonal coupling systems, such as SnoopCatcher/SnoopTag or biotin/streptavidin, could be explored for loading other antigens in our nanocarrier [23]. Their combination strategies can further be used to develop efficient multivalent vaccines. Another possible improvement is optimizing the vaccine administration route. Our results have shown that the nanovaccine without adjuvants stimulated efficient protection. This provides an opportunity for us to develop dissolving microneedle patches. Unlike current intramuscular injections, microneedle patches could deliver vaccines to the skin as an alternative pain-free method of vaccination. Moreover, immunization with microneedle patches does not require cold chain storage capacity and trained professionals, supporting their widespread use, especially in poor or developing countries where certain infectious diseases are highly prevalent.

Acknowledgments

This work was supported by the National Key Research and Development Program of China (2021YFC2102100), the National Natural Science Foundation of China (U20A20361, 32271507, 81930122, and 82171819), and the Beijing Postdoctoral Research Foundation (2021-ZZ-035).

Compliance with ethics guidelines

Jing Huang, Yufei Wang, Kangfeng Wang, Shulei Li, Peng Sun, Yan Guo, Jiankai Liu, Ruifu Yang, Ming Zeng, Chao Pan, Hengliang Wang, and Li Zhu declare that they have no conflict of interest.

Appendix A. Supplementary data

Supplementary data to this article can be found online at https://doi.org/10.1016/j.eng.2023.04.007.

References

[1] Pandey A, Cabello A, Akoolo L, Rice-Ficht A, Arenas-Gamboa A, McMurray D, et al. The case for live attenuated vaccines against the neglected zoonotic diseases brucellosis and bovine tuberculosis. PLoS Negl Trop Dis 2016;10(8):e0004572.

[2] Vishnu US, Sankarasubramanian J, Gunasekaran P, Rajendhran J. Identification of potential antigens from non-classically secreted proteins and designing novel multitope peptide vaccine candidate against *Brucella melitensis* through reverse vaccinology and immunoinformatics approach. Infect Genet Evol 2017;55:151–8.

[3] McDermott J, Grace D, Zinsstag J. Economics of brucellosis impact and control in low-income countries. Rev Sci Tech 2013;32(1):249–61.

[4] López-Santiago R, Sánchez-Argáez AB, De Alba-Núñez LG, Baltierra-Uribe SL, Moreno-Lafont MC. Immune response to mucosal *Brucella* infection. Front Immunol 2019;10:1759.

[5] Christopher S, Umapathy BL, Ravikumar KL. Brucellosis: review on the recent trends in pathogenicity and laboratory diagnosis. J Lab Physicians 2010;2(2):55–60.

[6] García-Méndez KB, Hielpos SM, Soler-Llorens PF, Arce-Gorvel V, Hale C, Gorvel JP, et al. Infection by *Brucella melitensis* or *Brucella papionis* modifies essential physiological functions of human trophoblasts. Cell Microbiol 2019;21(7):e13019.

[7] Ganesh NV, Sadowska JM, Sarkar S, Howells L, McGiven J, Bundle DR. Molecular recognition of *Brucella* A and M antigens dissected by synthetic oligosaccharide glycoconjugates leads to a disaccharide diagnostic for brucellosis. J Am Chem Soc 2014;136(46):16260–9.

[8] Sadeghi Z, Fasihi-Ramandi M, Azizi M, Bouzari S. Mannosylated chitosan nanoparticles loaded with FliC antigen as a novel vaccine candidate against *Brucella melitensis* and *Brucella abortus* infection. J Biotechnol 2020;310:89–96.

[9] Oliveira SC, Giambartolomei GH, Cassataro J. Confronting the barriers to develop novel vaccines against brucellosis. Expert Rev Vaccines 2011;10(9):1291–305.

[10] Pan C, Yue H, Zhu L, Ma GH, Wang HL. Prophylactic vaccine delivery systems against epidemic infectious diseases. Adv Drug Deliv Rev 2021;176:113867.

[11] Gomez G, Adams LG, Rice-Ficht A, Ficht TA. Host–*Brucella* interactions and the *Brucella* genome as tools for subunit antigen discovery and immunization against brucellosis. Front Cell Infect Microbiol 2013;3:17.

[12] Cassataro J, Pasquevich KA, Estein SM, Laplagne DA, Velikovsky CA, de la Barrera S, et al. A recombinant subunit vaccine based on the insertion of 27 amino acids from Omp31 to the N-terminus of BLS induced a similar degree of protection against *B. ovis* than Rev.1 vaccination. Vaccine 2007;25(22):4437–46.

[13] Rappuoli R. Glycoconjugate vaccines: principles and mechanisms. Sci Transl Med 2018;10(456):10.

[14] Peng Z, Wu J, Wang K, Li X, Sun P, Zhang L, et al. Production of a promising biosynthetic self-assembled nanoconjugate vaccine against *Klebsiella pneumoniae* serotype O2 in a general *Escherichia coli* host. Adv Sci 2021;8(14):e2100549.

[15] MacCalman TE, Phillips-Jones MK, Harding SE. Glycoconjugate vaccines: some observations on carrier and production methods. Biotechnol Genet Eng Rev 2019;35(2):93–125.

[16] Pan C, Sun P, Liu B, Liang H, Peng Z, Dong Y, et al. Biosynthesis of conjugate vaccines using an O-linked glycosylation system. MBio 2016;7(2):e00443–516.

[17] Sun P, Pan C, Zeng M, Liu B, Liang H, Wang D, et al. Design and production of conjugate vaccines against *S. Paratyphi A* using an O-linked glycosylation system *in vivo*. npj Vaccines 2018;3(1):4.

[18] Li X, Pan C, Liu Z, Sun P, Hua X, Feng E, et al. Safety and immunogenicity of a new glycoengineered vaccine against *Acinetobacter baumannii* in mice. Microb Biotechnol 2022;15(2):703–16.

[19] Huang J, Pan C, Sun P, Feng E, Wu J, Zhu L, et al. Application of an O-linked glycosylation system in *Yersinia enterocolitica* serotype O:9 to generate a new candidate vaccine against *Brucella abortus*. Microorganisms 2020;8(3):436.

[20] Gomes AC, Mohsen M, Bachmann MF. Harnessing nanoparticles for immunomodulation and vaccines. Vaccines 2017;5(1):5.

[21] Li X, Pan C, Sun P, Peng Z, Feng E, Wu J, et al. Orthogonal modular biosynthesis of nanoscale conjugate vaccines for vaccination against infection. Nano Res 2022;15(2):1645–53.

[22] Shi Y, Pan C, Wang K, Liu Y, Sun Y, Guo Y, et al. Construction of orthogonal modular proteinaceous nanovaccine delivery vectors based on mSA-biotin binding. Nanomaterials 2022;12(5):12.

[23] Brune KD, Howarth M. New routes and opportunities for modular construction of particulate vaccines: stick, click, and glue. Front Immunol 2018;9:1432.

[24] Dow JM, Mauri M, Scott TA, Wren BW. Improving protein glycan coupling technology (PGCT) for glycoconjugate vaccine production. Expert Rev Vaccines 2020;19(6):507–27.

[25] Ding J, Pan Y, Jiang H, Cheng J, Liu T, Qin N, et al. Whole genome sequences of four *Brucella* strains. J Bacteriol 2011;193(14):3674–5.

[26] Zhang Y, Li T, Zhang J, Li Z, Zhang Y, Wang Z, et al. The *Brucella melitensis* M5-90 phosphoglucomutase (PGM) mutant is attenuated and confers protection against wild-type challenge in BALB/c mice. World J Microbiol Biotechnol 2016;32(4):58.

[27] Li Z, Zhang J, Zhang KE, Fu Q, Wang Z, Li T, et al. *Brucella melitensis* 16MΔTcfSR as a potential live vaccine allows for the differentiation between natural and vaccinated infection. Exp Ther Med 2015;10(3):1182–8.

[28] Deqiu S, Donglou X, Jiming Y. Epidemiology and control of brucellosis in China. Vet Microbiol 2002;90(1–4):165–82.

[29] Jiang Y, Chen B, Duan C, Sun B, Yang J, Yang S. Multigene editing in the *Escherichia coli* genome via the CRISPR-Cas9 system. Appl Environ Microbiol 2015;81(7):2506–14.

[30] Bundle DR, McGiven J. Brucellosis: improved diagnostics and vaccine insights from synthetic glycans. Acc Chem Res 2017;50(12):2958–67.

[31] Yang K, Whalen BJ, Tirabassi RS, Selin LK, Levchenko TS, Torchilin VP, et al. A DNA vaccine prime followed by a liposome-encapsulated protein boost confers enhanced mucosal immune responses and protection. J Immunol 2008;180(9):6159–67.

[32] Avila-Calderón ED, Lopez-Merino A, Sriranganathan N, Boyle SM, Contreras-Rodríguez A. A history of the development of *Brucella* vaccines. BioMed Res Int 2013;2013:743509.

[33] Ghasemi A, Ranjbar R, Amani J. *In silico* analysis of chimeric TF, Omp31 and BP26 fragments of *Brucella melitensis* for development of a multi subunit vaccine candidate. Iran J Basic Med Sci 2014;17(3):172–80.

[34] Maione D, Margarit I, Rinaudo CD, Masignani V, Mora M, Scarselli M, et al. Identification of a universal group B *Streptococcus* vaccine by multiple genome screen. Science 2005;309(5731):148–50.

[35] Skwarczynski M, Toth I. Peptide-based synthetic vaccines. Chem Sci 2016;7(2):842–54.

[36] Yin D, Li L, Song D, Liu Y, Ju W, Song X, et al. A novel recombinant multi-epitope protein against *Brucella melitensis* infection. Immunol Lett 2016;175:1–7.

[37] He Y, Rappuoli R, De Groot AS, Chen RT. Emerging vaccine informatics. J Biomed Biotechnol 2010;2010:218590.

[38] Nazifi N, Tahmoorespur M, Sekhavati MH, Haghparast A, Behroozikhah AM. *In vivo* immunogenicity assessment and vaccine efficacy evaluation of a chimeric tandem repeat of epitopic region of OMP31 antigen fused to interleukin 2 (IL-2) against *Brucella melitensis* in BALB/c mice. BMC Vet Res 2019;15(1):402.

[39] Heidary M, Dashtbin S, Ghanavati R, Mahdizade Ari M, Bostanghadiri N, Darbandi A, et al. Evaluation of brucellosis vaccines: a comprehensive review. Front Vet Sci 2022;9:925773.

[40] Brune KD, Leneghan DB, Brian IJ, Ishizuka AS, Bachmann MF, Draper SJ, et al. Plug-and-display: decoration of virus-like particles via isopeptide bonds for modular immunization. Sci Rep 2016;6(1):19234.

[41] Chen Z, Zhu Y, Sha T, Li Z, Li Y, Zhang F, et al. Design of a new multi-epitope vaccine against *Brucella* based on T and B cell epitopes using bioinformatics methods. Epidemiol Infect 2021;149:e136.

[42] Sha T, Li Z, Zhang C, Zhao X, Chen Z, Zhang F, et al. Bioinformatics analysis of candidate proteins Omp2b, P39 and BLS for *Brucella* multivalent epitope vaccines. Microb Pathog 2020;147:104318.

[43] Singha H, Mallick AI, Jana C, Fatima N, Owais M, Chaudhuri P. Co-immunization with interlukin-18 enhances the protective efficacy of liposomes encapsulated recombinant Cu–Zn superoxide dismutase protein against *Brucella abortus*. Vaccine 2011;29(29–30):4720–7.

[44] Zhang H, Zheng H, Guo P, Hu L, Wang Z, Wang J, et al. Broadly protective $CD8^+$ T cell immunity to highly conserved epitopes elicited by heat shock protein gp96-adjuvanted influenza monovalent split vaccine. J Virol 2021;95(12):95.

[45] Pulendran B, Arunachalam PS, O'Hagan DT. Emerging concepts in the science of vaccine adjuvants. Nat Rev Drug Discov 2021;20(6):454–75.

[46] Yousefi S, Abbassi-Daloii T, Tahmoorespur M, Sekhavati MH. Nanoparticle or conventional adjuvants: which one improves immune response against Brucellosis? Iran J Basic Med Sci 2019;22(4):360–6.

[47] Fernandez-Prada CM, Zelazowska EB, Nikolich M, Hadfield TL, Roop 2nd RM, Robertson GL, et al. Interactions between *Brucella melitensis* and human phagocytes: bacterial surface O-polysaccharide inhibits phagocytosis, bacterial killing, and subsequent host cell apoptosis. Infect Immun 2003;71(4):2110–9.

[48] Eze MO, Yuan L, Crawford RM, Paranavitana CM, Hadfield TL, Bhattacharjee AK, et al. Effects of opsonization and gamma interferon on growth of *Brucella melitensis* 16M in mouse peritoneal macrophages *in vitro*. Infect Immun 2000;68(1):257–63.

[49] Abkar M, Lotfi AS, Amani J, Eskandari K, Ramandi MF, Salimian J, et al. Survey of Omp19 immunogenicity against *Brucella abortus* and *Brucella melitensis*: influence of nanoparticulation versus traditional immunization. Vet Res Commun 2015;39(4):217–28.

[50] Lin Y, He Y. Ontology representation and analysis of vaccine formulation and administration and their effects on vaccine immune responses. J Biomed Semantics 2012;3(1):17.

[51] Moran MC, Dominguez MP, Bence AR, Rodriguez MG, Goldbaum FA, Zylberman V, et al. Evaluation of the efficacy of polymeric antigen BLSOmp31 formulated in a new cage-like particle adjuvant (ISPA) administered by parenteral or mucosal routes against *Brucella ovis* in BALB/c mice. Res Vet Sci 2022;145:29–39.

[52] Haase S, Banerjee K, Mujeeb AA, Hartlage CS, Núñez FM, Núñez FJ, et al. H3.3-G34 mutations impair DNA repair and promote cGAS/STING-mediated immune responses in pediatric high-grade glioma models. J Clin Invest 2022;132(22):132.
[53] Salewski I, Kuntoff S, Kuemmel A, Feldtmann R, Felix SB, Henze L, et al. Combined vaccine-immune-checkpoint inhibition constitutes a promising strategy for treatment of dMMR tumors. Cancer Immunol Immunother 2021;70(12):3405–19.
[54] Lin MC, Lin YC, Chen ST, Young TH, Lou PJ. Therapeutic vaccine targeting Epstein-Barr virus latent protein, LMP1, suppresses LMP1-expressing tumor growth and metastasis *in vivo*. BMC Cancer 2017;17(1):18.
[55] Nezafat N, Karimi Z, Eslami M, Mohkam M, Zandian S, Ghasemi Y. Designing an efficient multi-epitope peptide vaccine against *Vibrio cholerae* via combined immunoinformatics and protein interaction based approaches. Comput Biol Chem 2016;62:82–95.
[56] Morici L, Torres AG, Titball RW. Novel multi-component vaccine approaches for *Burkholderia pseudomallei*. Clin Exp Immunol 2019;196(2):178–88.
[57] Arevalo CP, Bolton MJ, Le Sage V, Ye N, Furey C, Muramatsu H, et al. A multivalent nucleoside-modified mRNA vaccine against all known influenza virus subtypes. Science 2022;378(6622):899–904.
[58] Das A, Ali N. Nanovaccine: an emerging strategy. Expert Rev Vaccines 2021;20(10):1273–90.
[59] Mani S, Wierzba T, Walker RI. Status of vaccine research and development for *Shigella*. Vaccine 2016;34(26):2887–94.